Agricultural and Forest Meteorology 371 (2025) 110584

Contents lists available at ScienceDirect

Agricultural and Forest Meteorology

journal homepage: www.elsevier.com/locate/agrformet

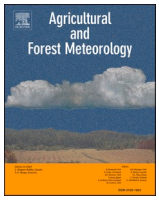

The Role of Atmospheric Boundary Layer Wind and Turbulence on Surface Pollen Levels

Juana Andújar-Maqueda [a,b], Pablo Ortiz-Amezcua [a,b], Paloma Cariñanos [a,c], Jesús Abril-Gago [a,b], Concepción De Linares [c], Gregori de Arruda Moreira [d], Juan Antonio Bravo-Aranda [a,b], María José Granados-Muñoz [a,b], Lucas Alados-Arboledas [a,b], Juan Luis Guerrero-Rascado [a,b,*]

[a] Andalusian Institute for Earth System Research (IISTA-CEAMA), University of Granada, Spain
[b] Department of Applied Physics, University of Granada, Spain
[c] Department of Botany, University of Granada, Spain
[d] Federal Institute of São Paulo, Registro, Brazil

ARTICLE INFO

Keywords:
Doppler lidar
ABL
turbulence
pollen
dispersion

ABSTRACT

The atmospheric boundary layer (ABL) is the lowest layer of the atmosphere, where most of the interactions between the atmosphere and the Earth's surface occur. Within this layer, the air movements and the turbulent processes facilitate the dispersion and transport of particles. This work quantifies the effect of ABL-dynamics related variables on the surface pollen concentrations in the city of Granada, southeastern Spain. The Main Pollen Season (MPS) of two pollen types (*Olea* and Cupressaceae) and Doppler lidar data for different height ranges and ABL regimes were used for the period 2017-2022 and statistically analyzed based on Spearman correlations and Generalized Linear Model (GLM). *Olea* pollen concentrations, mainly originating from sources in the outskirts of the city, were significantly influenced by daytime wind direction, transporting high concentrations into the urban area, explaining up to 28% of the variability of the *Olea* pollen concentrations in the ABL of the city. At night, surface *Olea* pollen concentrations were affected by vertical wind, which explain the 5% of the variability, leading to fluctuations associated with its vertical transport. For Cupressaceae pollen concentrations, however, the pollen sources are located within the city and surface concentrations of Cupressaceae pollen are predominantly influenced by the urban ABL. The variability in surface concentrations is partly determined by diverse phenomena and conditions occurring across different regimes of ABL dynamics. Katabatic flows significantly contributed to Cupressaceae pollen concentrations at night, while high turbulence produced by the convective boundary layer (CBL) played a key role in their dispersion during daytime, explaining up to 10% of the variability of the Cupressaceae pollen concentrations near to surface. The difference in the results between both pollen types can be attributed to several interrelated factors such as location of sources, local weather conditions, different ABL regimes, intrinsic characteristics of pollen, and the flowering phenology and interactions with other environmental factors. The overall results demonstrate the substantial influence of ABL dynamics on surface pollen concentrations (explain up to 29% of the variability for *Olea* pollen concentrations and 37% for Cupressaceae ones), highlighting its crucial role in the particle transport, dispersion and distribution in the atmosphere. These findings emphasize the need for a better understanding of the ABL to adequately address air quality and public health challenges in urban environments.

1. Introduction

Pollen grains are the most common type of primary biological airborne particles among the different categories of bioaerosols present in the atmosphere (Després et al., 2012; Fröhlich-Nowoisky et al., 2016). The pollen of anemophilous plant species has different sizes, ranging

* Corresponding author at: Juan Luis Guerrero-Rascado, Instituto Interuniversitario de Investigación del Sistema Tierra en Andalucía, Avenida del Mediterráneo, s/n, 18006, Granada, Spain.
E-mail address: rascado@ugr.es (J.L. Guerrero-Rascado).

https://doi.org/10.1016/j.agrformet.2025.110584
Received 19 June 2024; Received in revised form 26 March 2025; Accepted 21 April 2025
Available online 9 May 2025

from 5 to 100 μm, therefore considered as coarse mode particles. Their morphology is very variable, with different symmetries and multiple possibilities for their surface structure (Faegri et al., 1989). The duration of pollen suspension in the atmosphere is determined by these characteristics and, consequently, pollen grains can either remain in the vicinity of the source or be horizontally transported over different distances, ranging from a few meters to hundreds of thousands of kilometers (Griffin, 2007; Prospero et al., 2005; de Weger et al., 2016; Izquierdo et al., 2015; Frisk et al., 2022).

The presence of high pollen concentrations in the atmosphere is considered a form of biogenic pollution and is recognized as one of the major agents of allergy-related diseases such as asthma, rhinitis, and atopic eczema (Darsow et al., 1997; Naclerio, 1991; Zeldin et al., 2006). In the current context of climate change, the impact of pollen on human health is still more problematic, since it influences plant reproduction phenology (Schmidt, 2016; D'Amato et al., 2020; Choi et al., 2021). The ongoing climate changes are modifying the range of allergenic species and impacting the timing and length of the pollen season (Van Vliet et al., 2002; Frei et al., 2008), potentially increasing plant productivity and pollen production due to elevated carbon dioxide levels (Beggs, 2015). Moreover, the release and atmospheric dispersion of pollen is expected to be influenced by these climate-related changes, as highlighted by Bielory et al. (2012).

The pollen grains are released in the atmospheric boundary layer (ABL) and are expected to be affected by its dynamics. Wind and turbulence in the ABL are crucial for air quality, as they can disperse or transport aerosol particles from their sources and prevent their accumulation (Wei et al., 2020; Ren et al., 2021; Zhang et al., 2021). The vertical and horizontal distribution of aerosol particles is strongly influenced by the way the ABL disperses them. The dynamics of the ABL vary according to different regimes throughout the day. During daytime, the convective boundary layer (CBL) forms as a result of energetic turbulent movements caused by buoyant turbulence and turbulence generated by shear forces (Dosio et al., 2003; Liu et al., 2018). This dynamic regime facilitates thorough vertical mixing of aerosol particles within the ABL. During nighttime, turbulence and vertical mixing weakens and consequently a robust inversion often forms close to the surface because of the net radiative cooling. This inversion acts like a cap, trapping aerosols within the shallow nocturnal boundary layer (NBL) (Stull, 1988). As a result, it prevents the upward transport of aerosol particles into the free troposphere (Liu et al., 2020; Shi et al., 2021).

The influence of the ABL dynamics over the dispersion and transport of pollen grains has been rarely studied. On the one hand, having adequate knowledge of the spatial distribution of pollen grains in any place of interest, such as in urban areas or around emission areas, is a significant challenge due to the small number of pollen events analyzed, the lack of continuous measurements, the limitations in the vertical extent and the limited number of aerobiological stations (e.g. Santiago et al., 2013; Borycka and Kaprzyk, 2018). On the other hand, there are studies that investigate the relationship between the daily cycle of pollen emission and standard surface meteorological variables such as temperature, relative humidity, solar radiation, atmospheric pressure, accumulated precipitation and wind speed and direction (e.g. Majeed et al., 2018; Cariñanos et al., 2022). However, they are limited to variables measured near the surface. In the last decades, some studies have investigated the dispersion of bioaerosol particles using numerical simulations to model the ABL dynamics (e.g. Kuparinen et al., 2007; Robichaud and Comtois, 2021; Roy et al., 2023), but these simulations should be supported by empirical measurements to improve their predictive ability and accuracy.

The exploration of turbulent behavior of the ABL is relevant as this process might impact the transport of bioaerosol particles, with sources including buoyancy and wind shear production, which are highly variable in time and space. In this context, Doppler lidars can be used to retrieve the 3D wind field and turbulent properties within ABL, which can provide a classification of turbulence based on its source (Manninen et al., 2018). So far, lidar-based pollen studies have analyzed the different optical properties of this aerosol type (e.g. Córdoba-Jabonero et al., 2018; Shang et al., 2020; Veselovskii et al., 2021; Shang et al., 2022). For example, a study carried out by Sicard et al. (2016) explores correlations between depolarization ratios, pollen concentrations and solar fluxes, revealing insights into the monitoring of pollen release and the influence of atmospheric turbulence on particle motion. During pollination events in Finland, lidar measurements revealed the potential of particle depolarization ratio to track pollen grains in the atmosphere (Bohlmann et al., 2021), or the spectral dependence of optical properties for different pollen types (Filioglou et al., 2023). It is noteworthy that the exploration of the dynamics of the ABL concerning surface pollen levels has been underexplored in previous research.

This study aims to fill this research gap by investigating the impact of the ABL dynamics on surface pollen concentrations during periods of significant concentration of the most predominant pollen types in the atmosphere of a representative medium-sized mediterranean city, Granada, southeastern Spain. To this end, extensive datasets of surface pollen concentration obtained through volumetric suction Hirst sampler along with variables related to the ABL dynamics and turbulent processes measured by a Doppler lidar have been analysed with different statistical tools. The goal is to offer a thorough comprehension of the behavior of the pollen grains concentrations during their transport and dispersion within ABL under different conditions, as well as quantify the influence of the ABL dynamics during these processes.

2. Experimental site and instrumentation

2.1. Climate and Pollen Conditions in Granada

The study was carried out for Granada, Spain (37.18° N, 3.61° W, 680 m asl), a city located in a closed depression crossed by the river Genil. Granada covers an area of 88.02 km^2 and had a population of 230,595 in 2023. It is bordered by mountain ranges, notably Sierra Nevada, which contains the highest peak in the Iberian Peninsula at over 3,400 m a.s.l., located 40 km southeast of the city. The climate is characterised by significant seasonal temperature variations, with an average winter temperature of 2°C and an average maximum summer temperature of 33°C, and low annual rainfall, with an average of 352 mm, resulting in a relatively dry environment (annual relative humidity of 57%), according to AEMET (2024). The average surface wind speed is low at 2 m s^{-1}, with night winds prevailing from the SE and day winds prevailing from the N. However, between 100 and 580 m a.g.l., the wind field shows a predominance of NW winds during the day, shifting to E-SE at night, indicating a katabatic flow as cooler and denser air descends from the Sierra Nevada into the valley (Montávez et al., 2000; Ortiz-Amezcua et al., 2022).

Granada is surrounded by significant natural spaces, including the national park of Sierra Nevada, as well as agricultural areas in close proximity of the city. The atmosphere of the region contains a rich diversity of pollen types from various ecosystems, including mountain areas with grasslands, holm oaks (*Quercus* spp.), junipers (*Juniperus* spp.), pine forests (*Pinus sylvestris, P. nigra*) (De Linares et al., 2017), olive groves (*Olea europaea* var. *sylvestris*), and cereal crops (Poaceae). Additionally, pollen from urban trees located in the green areas of the city is prevalent, with the most frequent genera being cypress (*Cupressus* spp.), plane tree or sycamore (*Platanus x hispanica*), poplar (*Populus* spp.), maple (*Acer* spp.), elm (*Ulmus* spp.), and ash (*Fraxinus* spp.) (Díaz de la Guardia et al., 2006; Cariñanos et al., 2014, 2016a). Within the variety of pollen types found in the atmosphere of the city, the most predominant are *Olea* and Cupressaceae during their respective peak emission periods (Alba et al., 2000). *Olea* accounted for 36% of the total atmospheric pollen of the city, and Cupressaceae accounted for 30% between 1992 and 2018 (Cariñanos et al., 2021). This predominance highlights our decision to focus our research on these two pollen types.

The pollen grain of *Olea* is trizonocolporate, isopolar and radiosymmetric, sub-circular lobed, reticulate, and of medium to small size, 20-29 μm. Its flowering season is mainly spring, and flowering in the Mediterranean region can extend from the months of March to early July, following a latitudinal and altitudinal gradient (Trigo et al., 2008). There are numerous studies that confirm the regional and very long-distance transfer from its emission sources (Negral et al., 2021).

The pollen type of Cupressaceae is shared by all genera belonging to this family and those of related families such as Taxaceae. The pollen grain is inaperturate, apolar and radiosymmetric, spheroidal, psilat bis scabrat, with a size between 20-30 μm. It is a very light pollen grain, with a fragile exine that fractures easily. Given the numerous species included in this family, flowering can occur throughout the year, although many of them flower mainly in winter (Trigo et al., 2008). It is a very light pollen and there is evidence from molecular and trajectory analyses that confirm the long-distance transport of pollen emitted in localities in Oklahoma (USA) to locations in the state of Ontario (Canada) (Mohanty et al., 2017).

The main source of *Olea* pollen, olive groves, are located in the outskirts of the city, with a greater extension and a greater proximity to the North and Northeast of the city, as they border the city limits (Fig. 1a). A large number of areas dedicated to olive cultivation can also

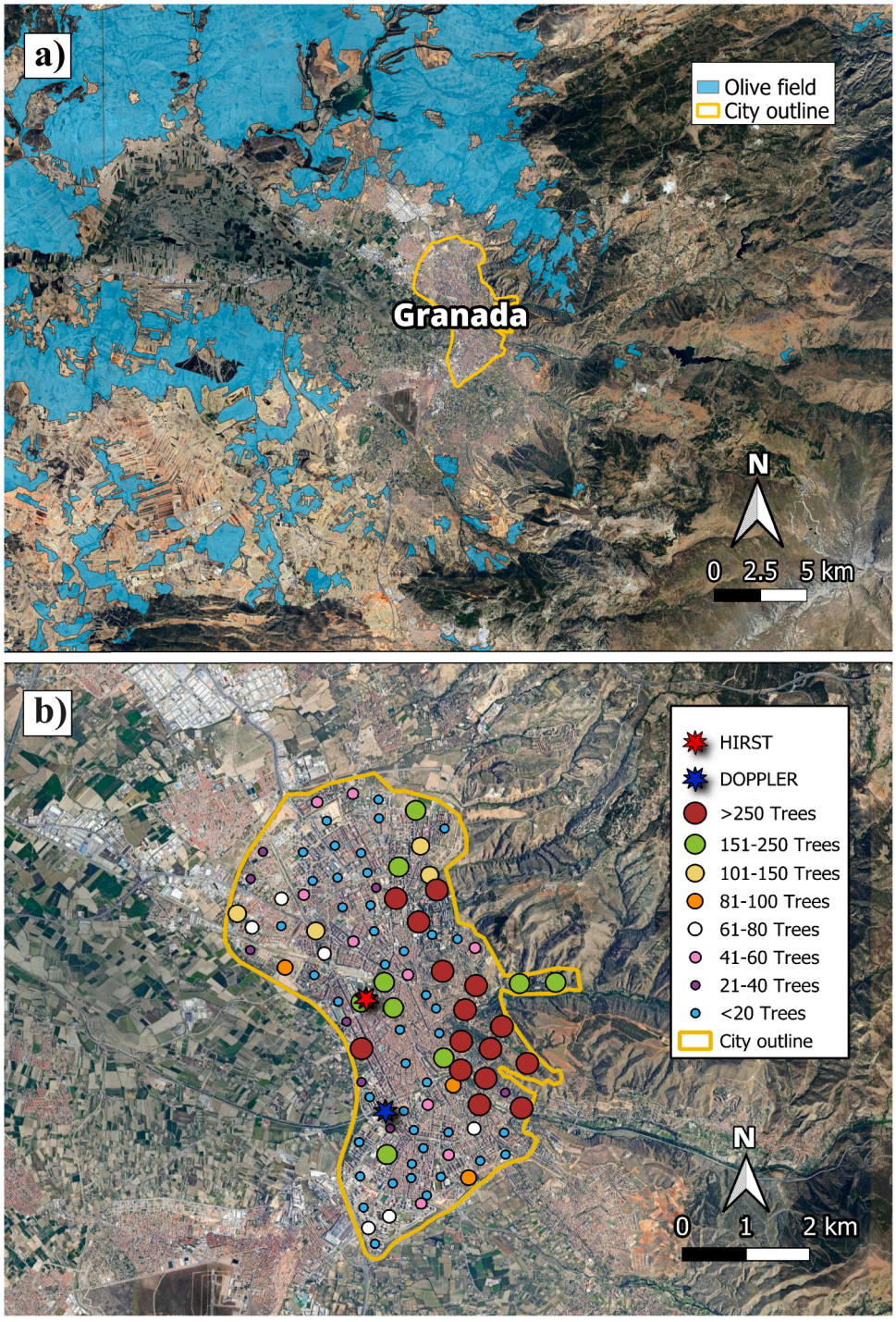

Fig. 1. Distribution of a) irrigated olive groves located around the city of Granada (Data source: Andalusian Spatial Reference Data (DERA), provided by the Andalusian Institute of Statistics and Cartography (IECA)) and b) cypresses trees within the city of Granada (adapted from López and Cariñanos, 2020).

be observed to the Northwest and West, however in this case they are several kilometers away from the city. To the Southwest there are also small olive groves distributed in a more dispersed manner. In the Southeast quadrant, the Sierra Nevada mountain range prevents the presence of significant olive growing areas.

The sources of the Cupressaceae pollen are found within the city limits. Fig. 1b illustrates that cypress trees are distributed throughout the entire city, although the distribution is neither uniform nor homogeneous. A higher concentration of cypresses can be seen in the eastern side of the city with a large number of locations marked as areas where more than 250 cypresses are found. In other areas of the city, the density of these trees is lower, with some locations having a substantial number of cypresses, but more spread out (Cariñanos et al., 2016b).

2.2. Aerobiological data

Daily airborne pollen counts of pollen types of interest were provided using the dataset of pollen recorded at the Unit of the Biological Air Quality of the University of Granada. Aerobiological data are collected from a Hirst-type volumetric sampler (Hirst, 1952) Lanzoni VPPS 2000 (Lanzoni, s.r.l., Bologna, Italy). The instrument sucks in the air through a narrow inlet, which is aligned with the air direction by a weather vane. The sampler collects all that is in the air (such as pollen grains, spores, dust and small insects) which is then impacted on a silicon-coated Melinex tape moved across the orifice at a rate of 2 mm/h. Each week the tape is collected and divided into segments corresponding to the days of the year. It is subsequently analyzed under an optical microscope for counting and classifying pollen grains daily, with a minimum analyzed sample percentage of 10% recommended as a requirement by the European Aeroallergen Network (Galán et al., 2014) and the Spanish Aerobiology Network (REA) in its Quality and Management Manual (Galán et al., 2007). This recommendation considers both the number of longitudinal traverses conducted and the diameter of the microscope's field of view. Although statistical errors during the slide reading process (Comtois et al., 1999) and human errors in counting and identifying pollen grains can vary based on observer skill and sample complexity (Gottardini et al., 2009), the methodology used is standardized and can be compared with the scientific literature. The sampler is located on the roof of the Faculty of Sciences of the University of Granada (37.18° N, 3.61° W, 680 m a.s.l.), located in the center of the city (Fig. 1b), at a height of 20 m above ground level.

2.3. Doppler Lidar StreamLine system

The Doppler lidar system consists of a pulsed laser system emitting at a wavelength of 1.5 μm and a heterodyne detector using optical-fiber technology. Emission is produced with an energy pulse of 100 μJ and a high pulse repetition rate of 15 kHz. More technical details about the instrument can be found in Ortiz-Amezcua et al. (2022). The 3D wind field and turbulent properties of the ABL were obtained using the measurements of the Doppler lidar StreamLine (HALO Photonics), that is part of ACTRIS-CCRES (https://www.actris.eu/facilities/national-facilities/observational-platforms, last access: 3 June 2024), previously Cloudnet (Illingworth et al., 2007) operated by the Atmospheric Physics Group (GFAT) of the University of Granada. This system is located at the UGR station, part of the AGORA facility (Andalusian Global Observatory of the Atmosphere), within the Andalusian Institute for Earth System Research (IISTA-CEAMA) of the University of Granada (Fig. 1b). This station is part of several instrumental and research networks as well as of ACTRIS (Laj et. al., 2024).

Some instrumental parameters can be modified. For this study, the instrument operated with a vertical resolution of 30 m with an effective range from 90 m to 6000-9000 m and a temporal resolution of around 2 s. Initially, the focal length of the optical system was 535 ± 35 m, determined experimentally using the method described in Pentikäinen et al. (2020), which increases the instrument sensitivity at this altitude but decreases it above 2 km. Later, in June 2021, the instrument was upgraded and the focus was set to infinity, improving its sensitivity at higher altitudes. The signal acquisition was continuous and autonomous pointing vertically (stare mode) combined with a conical scan repeated every 10 min with an elevation of 75° and 12 equidistant azimuth points. The study period spans from 2017 to 2022.

3. Methodology

3.1. Surface pollen levels

The temporal series of the surface pollen concentrations for *Olea* and Cupressaceae for each study year are shown in Fig. 2. The daily counts of Cupressaceae pollen show high concentrations during the first months of each year, while for the case of the *Olea*, the maximum pollen period is observed in the spring and early summer months. There are gaps in the data, attributed to the instrument's non-operational status. Only Main Pollen Season (MPS) days were considered for statistical analysis. The MPS was determined by applying the 95th percentile method to the pollen data set (Goldberg et al., 1988) for each pollen type and year of study. This method establishes that the start of the MPS occurs when 2.5% of the total annual pollen count has been recorded, and the end of this period, when 97.5% of the total annual pollen count has been recorded. Additionally, MPS days with a null or low concentration, i.e. less than 50 pollen grains m^{-3} of air (Galán et al., 2007), were excluded. This approach helps to avoid periods of low or negligible pollen emissions, which would not provide useful information for this study. This pollen exclusion threshold in both pollinic types was realised following the recommendation of the Spanish Aerobiology Network (REA), which considers that *Olea* and Cupressaceae register similar Annual Pollen Integral, Daily pollen levels and, allergic potential (Galán et al., 2007). Consequently, the analysis includes a total of 229 days (i.e. pairs of data points) for Cupressaceae pollen type and 87 days for *Olea* pollen type.

The effect of rainfall has not been considered in the data analysis, as the extensive historical aerobiological database in Granada have shown that rainfall only significantly affects pollen levels when sustained and exceeding 10 mm per day. It has also been observed that rainfall impacts herbaceous species more than arboreal ones, leading to a less pronounced response in the studied arboreal pollen types.

3.2. ABL turbulent properties and 3D wind field

The turbulent variables and the 3D wind field related to the ABL dynamics were obtained from Doppler lidar measurements processed with the software package HALO lidar toolbox (Manninen, 2019). The purpose of this software is to derive harmonized Doppler lidar retrievals applied to measurements from different sites using robust methods and providing consistent uncertainty estimates. This software is based on estimating the attenuated backscatter from the signal intensity, as well as estimating the statistical moments of vertical velocity as a starting point for the turbulence classification. The attenuated backscatter coefficient (β_{att}) refers to the backscatter of aerosol particles, adjusted for the attenuation of radiation in the atmosphere between the Doppler lidar and the volume of interest.

The variables related to the ABL dynamics and their estimation method in the HALO lidar toolbox processing chain are detailed below:

- **3D wind field, v_h, *dir* and *w*:** The 3D wind field and its associated errors are calculated from conical scans at 75° elevation using Velocity-Azimuth Display (VAD) technique (e.g. Päschke et al., 2015; Newsom et al., 2017). The three wind components are estimated, namely *u*-component (zonal component or west-east direction), *v*-component (meridional component or south-north direction) and *w*-component (*w*, vertical component). The horizontal wind is also given in terms of wind speed (v_h) and direction from where the wind blows (*dir*, clockwise starting from north). For the data analyzed in

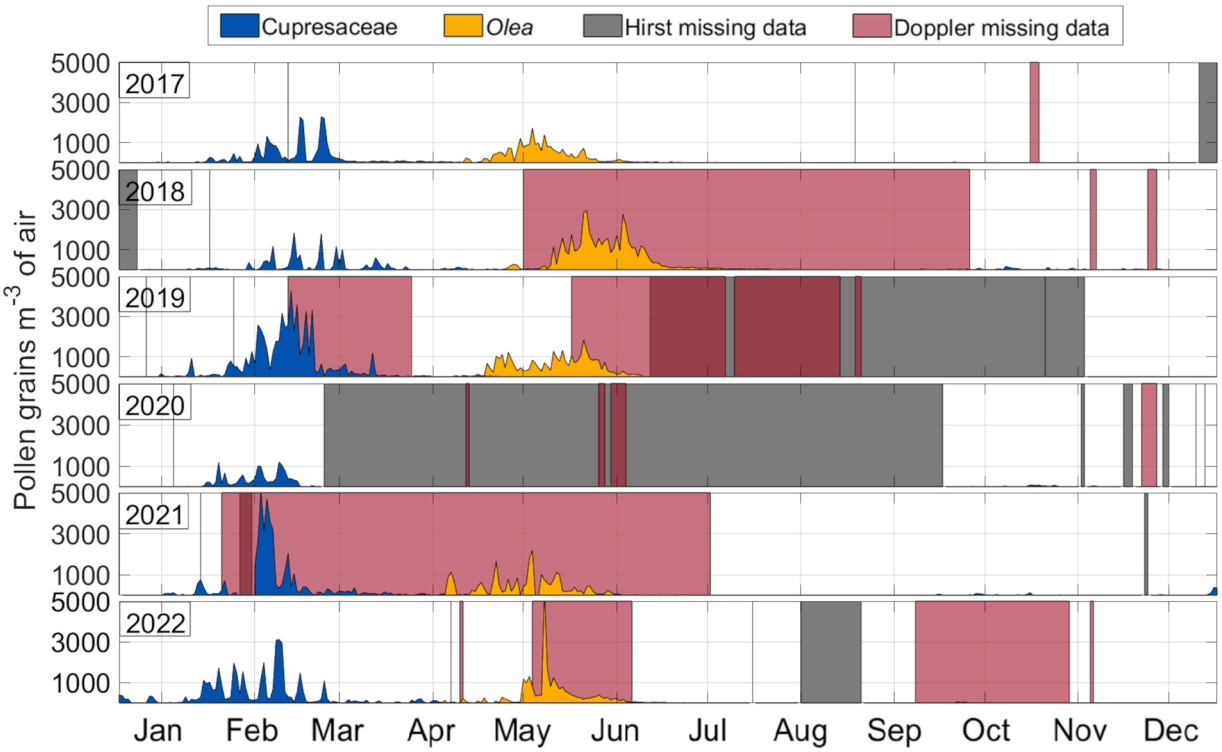

Fig. 2. Pollen concentration series of Cupressaceae (in blue) and *Olea* (in yellow) during the selected study period (2017-2022). Days without pollen data are indicated in gray, while days without Doppler lidar data are highlighted in red. The overlapping days with no data from both the Hirst and Doppler lidar appear in dark red.

this study, the mean error for the obtained v_h and w are 0.50 and 0.09 m s^{-1}, respectively. Additionally, the mean error for *dir* is 0.52°.

- **Turbulent kinetic energy dissipation rate, ε:** This variable is defined as the rate at which turbulent kinetic energy is absorbed by eddies which are divided into smaller eddies until they are finally dissipated into heat by viscous forces (Garrat, 1994) according to the hypothesis of Kolmogorov (1941). This variable informs of the existence of turbulence in a given atmospheric region. It is estimated according to the method of O'Connor et al. (2010):

$$\varepsilon = 2\pi \left(\frac{2}{3a}\right)^{3/2} \sigma_w^3 \left(L^{2/3} - {L_1}^{2/3}\right)^{-3/2} \quad (1)$$

where $a = 0.55$ is the Kolmogorov constant, σ_w is the standard deviation of the mean vertical wind speed (with 2 s time resolution) for a given time interval (30 min), L is the length scale of the largest eddies that pass completely through the laser beam, and L_1 is the length scale describing the beam scattering volume for an individual sample. To obtain L and L_1, it is necessary to use the wind speed obtained from the VAD scans performed by the Doppler lidar. L and L_1 are defined as follows:

$$L_1 = v_h t + 2z\, sin\left(\frac{\theta}{2}\right) \quad (2)$$

$$L = N v_h t \quad (3)$$

where θ corresponds to the divergence angle of the laser beam, v_h is the horizontal wind speed (obtained each 10 min), t is the time configured to acquire a wind speed profile using the Doppler lidar system (2 s), z is the height, and N is the number of samples. Typically, the second term of Eq. (2) can be neglected for Doppler lidar instruments due to their very small divergence (<0.1 mrad).

The presence of turbulence is detected with the threshold value of $\varepsilon > 10^{-4}$ m^2 s^{-3} (e.g., Borque et al., 2016; Vakkari et al., 2015). The method also provides the error estimate of ε, described in terms of the fractional error $\Delta\varepsilon/\varepsilon$, $\Delta\varepsilon$ is the absolute error of ε (for more details, see O'Connor et al., 2010). For the data analyzed in this study, the mean error obtained for ε is 76%.

- **Wind shear, *sh*:** Horizontal wind shear is the rate of change of wind speed and direction between two points of different altitude Δz. It is a source of turbulence and can be calculated from Doppler lidar measurements of the horizontal wind components. The estimated wind shear vector is calculated with the following expression:

$$sh = \frac{(\Delta u^2 + \Delta v^2)^{1/2}}{\Delta z} \quad (4)$$

In our case the wind shear vector is calculated for height ranges of $\Delta z = 90$ m. The uncertainty of the wind shear vector is obtained by error propagation of its component variables, i.e. by the wind components u and v. The threshold value for this variable to be considered as producing turbulence within the ABL is $sh > 0.03$ s^{-1} (Manninen et al., 2018). For the wind shear data analyzed in this study, the mean error obtained for *sh* is 0.01 s^{-1}.

3.3. Data preparation for analysis or data reduction

Our study involved the use of two databases with different temporal resolution, i.e. one from Doppler lidar (3 min for turbulence variables and 10 min for wind variables) and the other related to pollen measurements (daily temporal resolution). In order to carry out the relevant statistical studies and examine the relationship between them, the daily pollen concentration values are considered representative of the 24-h period. Doppler lidar data are grouped and averaged for three different periods (i.e. *all day, convective* and *non-convective* conditions) and three different altitude ranges. Since the extent range of the Doppler lidar system is limited, with values up to 1500 m in high aerosol loading conditions and approximately 500-1000 m in low aerosol loading

conditions, the study does not consider heights above 500 m. The height ranges that were analyzed were 90 to 150 m, 90 to 250 m, and 90 to 500 m, thus capturing the behavior of each of the variables in the different study ranges of the ABL. Each day was also divided into three intervals, one of which represented the whole day (*all day* period), and the other two periods were selected according to the two different ABL regimes that occur throughout the day, i.e. the CBL, during daytime (*convective* period), and the stable boundary layer (SBL) at nighttime (*non-convective* period). Given the unknown emission pattern of pollen throughout the day, the division of the ABL into various scenarios was designed to capture the influence of different ABL conditions on total daily pollen concentrations, focusing on how both *convective* and *non-convective* periods of each day can affect the corresponding daily accumulated surface pollen concentration. The *convective* scenarios investigate how the mean ABL conditions during daytime influence the total daily pollen concentrations. The *non-convective* scenario studies how the mean ABL conditions during nighttime influence the same daily accumulated pollen concentrations. Lastly, *all day* periods study how the mean ABL conditions throughout the entire day influence the same daily accumulated pollen concentrations. The *convective* and *non-convective* periods were calculated from an ABL classification according to the turbulent mixing source (Manninen et al., 2018). This classification labels a data point as convective mixing when the β_{att} is less than 10^{-5} sr^{-1} m^{-1} (otherwise, it would be labelled as cloud), the skewness of the vertical velocity is positive (indicating ascending air masses), turbulence exceeds a threshold of $\varepsilon > 10^{-4}$ m^2 s^{-3} and is connected to the surface during daytime hours. Periods characterized by the presence of convective mixing were designated as *convective*, while the remaining hours of the day were classified as *non-convective*.

Therefore, the mean of each variable was calculated for all study scenarios. These scenarios included all combinations of the selected height ranges in the ABL and the different periods of the day. In this way, each daily pollen concentration was associated with nine distinct scenarios, harmonizing with the daily pollen dataset and allowing us to examine the influence of each combination.

3.4. Statistical analysis

An initial characterization of the pollen sources was conducted with the use of bivariate plots for each pollen type and study scenario. These representations illustrate the average pollen concentration (indicated by a color scale) in relation to specific wind speeds (represented on a radial scale) and directions. In both *convective* and *non-convective* scenarios, the 24-h surface pollen concentrations are analyzed with respect to the prevailing wind during daytime and nighttime, respectively.

To investigate potential monotonic relationships between the aerobiological data and each continuous variables obtained from the Doppler lidar system, Spearman correlation was employed. This allowed for assessing whether there was a significant relationship by examining the presence of increasing (or decreasing) associations in the data. Wind direction was excluded from all Spearman analyses in this study due to its cyclic nature.

The research was then extended by considering each of the dynamic and turbulent variables jointly through the application of Generalised Linear Models (GLMs). GLMs are widely used in a number of different fields of knowledge such as ecology (e.g. del Águila et al., 2024), medicine (e.g. Dominici et al., 2005), neuroscience (e.g. Alarefi et al., 2022), environmental science (e.g. Charalampopoulos et al., 2018) and economy (e.g. Egger and Staub, 2016). These are an extension of traditional linear models and allow for dealing with situations where the relationship between variables is not necessarily linear or the distribution of the data does not follow a normal distribution.

In the context of this study, the GLM with logarithmic link function was applied to model the behavior of surface pollen concentrations (response variable) which present a negative binomial distribution, incorporating variables associated with ABL dynamics as explanatory variables into the model. Integrating these variables into the model provides insight into the magnitude and direction of their impact on pollen levels, considering both their independent and joint contribution. The problem of the non-linearity of the wind direction can be resolved by transforming it into a categorical variable. Unlike numerical variables representing continuous quantities, categorical variables divide data into distinct groups or categories (e.g. Silva, 2014; Santos-Alamillos et al., 2015; Rachmawati et al., 2021). The full range of wind directions was divided into eight categories, each spanning an angular sector of 45°.

In order to obtain unbiased model coefficient estimates and significance it is necessary to avoid multicollinearity among the explanatory variables, i.e. that they are not highly correlated with each other. To detect multicollinearity, a method based on the sample correlation between explanatory variables was applied, which consists of calculating the so-called Variance Inflation Factors (VIFs). Collinearity will exist when the explanatory variable presents a VIF > 5 (e.g. Wahid et al, 2021; Saha et al, 2022; Janizadeh et al., 2023). Additionally, to assess the goodness of the GLMs fit, a chi-squared goodness-of-fit test was conducted. To further enhance model accuracy, Cook's distance (Cook, 1979), a statistical measure used to identify influential observations and potential outliers, was calculated for each GLM model. Observations with distances exceeding $4/n$, where n represents the number of observations (e.g. Weichle et al., 2013; Halt et al., 2015; Guitart-Masip et al., 2016), were removed from the model, constituting less than 10% of the total observations. These exclusions corresponded to anomalous days characterized by atypical behavior of some variables.

The sign of the estimated model coefficients for each explanatory variable, along with their statistical significance, are presented as the results of GLMs, indicating if a certain variable affects positively or negatively to the increase of daily pollen concentration. The estimated coefficients from the GLM output have been omitted from the results because their magnitude depends on the variable itself, not making them comparable among the different variables in the model. Instead, the reduction in D^2 obtained from the ANOVA test provides a more representative measure of the contribution of each variable to the model, allowing for a more consistent evaluation of their effects.

Furthermore, the model output includes the variance explained by the model (D^2) which is computed from residuals of the null model and the fitted model. The coefficient D^2 represents the proportion of variance in the dependent variable that can be explained by the explanatory variables in a model. In other words, it indicates how effectively the selected variables account for fluctuations in pollen concentration. This is an important output to consider, as it provides insights into the overall explanatory power of the model. Additionally, a type II ANOVA test was conducted to determine whether the inclusion of each explanatory variable significantly enhances the ability of the model to explain observed variability (e.g. Ahmed et al., 2017; Hurtado et al., 2020; Zhou et al., 2023). A p-value < 0.05 suggests that a variable is statistically significant, and its inclusion improves the model fit. This test also shows the reduction in D^2 of the model when each of the variables is omitted. It is important to consider that the sum of the reductions in D^2 of all variables obtained from the ANOVA tests does not necessarily equal the D^2 of the GLM model. The variables may interact with one another, meaning that the D^2 by the combination of two variables in the model can be different the sum of their individual reductions in D^2. This occurs because their interaction generates a combined effect that is only captured through their joint consideration in the analysis.

4. Results

4.1. Olea

4.1.1. Olea pollen sources

During the *Olea* MPS, a large concentration of pollen grains is registered near the surface, although the trees are not abundant in the

city. To identify the most important sources of *Olea,* Fig. 3 presents the bivariate polar plots corresponding to different scenarios.

It can be observed that regardless of height range, very similar situations occur for *all day* and *convective* periods, indicating the predominance of the *convective* conditions along the day and homogeneous wind properties with height. High concentrations of *Olea* pollen with more than 700 pollen grains m^{-3} on average are detected for W and NW winds of more than 4 m s^{-1}. For *non-convective* or nocturnal periods, the days when higher total concentrations were registered show the prevalence of nocturnal winds from W-NW, again observing an advection of *Olea* pollen grains from these directions. However, in this case the transport appears more moderate with concentrations around 600 pollen grains m^{-3} on average with wind speeds around 4-5 m s^{-1}. It is noteworthy that all directions present a contribution of *Olea* pollen grains for low wind speeds (lower than 4 m s^{-1}), with a contribution of 500 *Olea* pollen grains m^{-3} from the W sector and 300 pollen grains m^{-3} from E sector on average.

4.1.2. Spearman correlations for Olea

The impact of *w* becomes evident through a statistically significant negative correlation observed for *all day* periods in the lower height ranges and for *non-convective* periods in all the altitude ranges (Table 1). The values of the correlation coefficients are between -0.22 and -0.31, being higher to the height range from 90 to 150 m. This variable presents no correlation in the *convective* period.

The rest of the analyzed variables are not significantly correlated with the *Olea* pollen concentration. Hence, there is no monotonic relationship between the v_h, ε and *sh* of the urban ABL and the *Olea* pollen concentrations near the surface.

4.1.3. GLMs for Olea

The large influence of *dir* on *Olea* pollen concentrations at the surface is observed in Table 2. This variable is statistically significant in all scenarios at any height range. During *all day* periods and any height range, S, SW, W and NW directions show a positive coefficient in the model which indicating an increase of *Olea* pollen concentrations, with NE also contributing to the height range between 90-500 m. The situation changes for *convective* periods, where only the NW direction shows a positive effect while the S and SW directions display a negative effect for any height range. For *non-convective* periods, as altitude increases, the number of statistically significant wind directions rapidly decreases. Regardless of the height range, all these wind directions show a positive effect on *Olea* pollen concentrations. Variable *w* is statistically significant, but only during the *non-convective* periods in the lowest and highest height ranges where it shows a negative effect on *Olea* pollen concentrations.

D^2 of each model ranges from 16% to 29% depending on the study scenario (Table 2), values comparable to previous studies (e.g. Kasprzyk et al., 2014; Cariñanos et al., 2020). In *all day* periods, the percentages for all height ranges remain close around 27%. According to the ANOVA test (Table 3), the variable *dir* is responsible for most of these percentages. The D^2 of the model is not significantly influenced by the rest of the variables. For *convective* periods, the highest D^2 of all *Olea* models is found for the height range from 90 to 500 m (Table 2). As above, the *dir* is able to explain almost the entire D^2 for each model with values up to 27% for the height range from 90 to 500 m. During *non-convective* periods, the percentages of D^2 decrease for larger height ranges. In addition, according to the ANOVA test, the influence of *dir* also decreases with the height, showing no statistical significance in the highest height

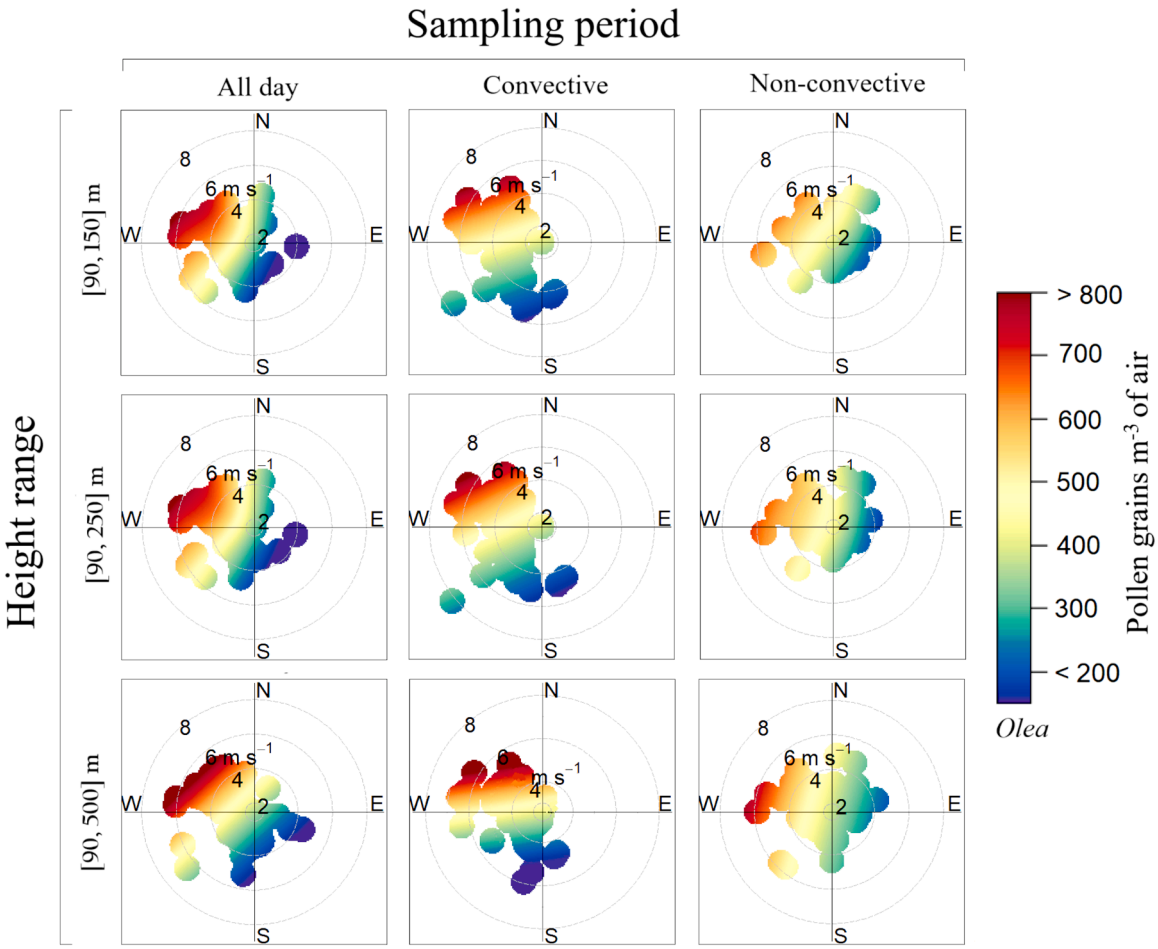

Fig. 3. Bivariate polar plots for the *Olea* pollen type at different height ranges and sampling periods. Circles represent horizontal wind speed in m s^{-1}.

Table 1
Spearman correlation coefficients between *Olea* daily pollen concentrations and each of the selected variables associated with the ABL dynamics for different height ranges and ABL regimes. Only statistical significant coefficients, i.e. those with a p-value < 0.05, are shown.

	Olea [90, 150] m				*Olea* [90, 250] m				*Olea* [90, 500] m			
	v_h	*w*	ε	*sh*	v_h	*w*	ε	*sh*	v_h	*w*	ε	*sh*
All day	-	-0.29	-	-	-	-0.22	-	-	-	-	-	-
Convective	-	-	-	-	-	-	-	-	-	-	-	-
Non-convective	-	-0.31	-	-	-	-0.22	-	-	-	-0.27	-	-

Table 2
Sign of the coefficient estimates of the linear predictor when applying a GLM model with *Olea* pollen as the response variable and the selected parameters associated with the ABL dynamics as the explanatory variables for different height ranges and ABL regimes. Only statistical significant coefficients, i.e. those with p < 0.05 (*), p < 0.01 (**) and p < 0.001 (***) are presented. The percentage of variance explained (D^2) of each model is also included.

	v_h	*w*	ε	*sh*	*dir*								D^2 (%)
					N	NE	E	SE	S	SW	W	NW	
							***Olea* [90, 150] m**						
All day	-	-	-	-	-	-	-	-	(+)*	(+)**	(+)**	(+)***	27.49
Convective	-	-	-	-	-	-	-	-	(-)***	(-)**	-	(+)***	20.91
Non-convective	-	(-)*	-	-	(+)***	(+)***	(+)**	(+)***	(+)*	(+)*	(+)***	(+)**	26.19
							***Olea* [90, 250] m**						
All day	-	-	-	-	-	-	-	-	(+)*	(+)**	(+)**	(+)***	27.10
Convective	-	-	-	-	-	-	-	-	(-)***	(-)**	-	(+)***	16.87
Non-convective	-	-	-	-	-	(+)**	(+)**	(+)***	(+)**	(+)***	(+)***	(+)***	20.56
							***Olea* [90, 500] m**						
All day	-	-	-	-	-	(+)**	-	-	(+)***	(+)***	(+)***	(+)***	27.50
Convective	-	-	-	-	-	-	-	-	(-)***	(-)**	-	(+)***	28.63
Non-convective	-	(-)**	-	-	-	-	-	-	-	-	(+)***	-	15.92

Table 3
Percentage of D^2 contributing to the model each of the selected variables related to the ABL dynamics obtained by a type II ANOVA test applied to each GLM model. Significance code: p < 0.05 (*), p < 0.01 (**) and p < 0.001 (***).

	Olea [90, 150] m					*Olea* [90, 250] m					*Olea* [90, 500] m				
D^2 (%)	v_h	*w*	ε	*sh*	*dir*	v_h	*w*	ε	*sh*	*dir*	v_h	*w*	ε	*sh*	*dir*
All day	0.28	1.84	1.00	1.16	**18.47** ***	0.01	0.50	3.07	0.60	**22.92** ***	0.30	1.38	1.95	0.00	**23.03** ***
Convective	1.23	0.14	0.25	1.81	**18.52** ***	0.02	0.03	0.57	0.06	**15.89** ***	0.04	0.00	2.42	0.26	**27.13** ***
Non-convective	1.35	**5.07** *	0.02	0.24	**18.20** ***	2.61	1.75	0.62	1.32	**14.99** ***	0.00	**5.36** ***	0.03	1.23	9.96

range. However, it is also important to consider the statistical significance of *w* during this period of the day, explaining over 5% of variability of *Olea* pollen concentrations at surface in both height ranges, from 90 to 150 m and 90 to 500 m.

4.2. Cupressaceae

4.2.1. Cupressaceae pollen sources

In order to identify the main sources of the Cupressaceae pollen type in the city of Granada, Fig. 4 shows the Cupressaceae pollen bivariate polar plots for different height ranges and ABL regimes.

For *all day* and *non-convective* periods, the average concentrations from SE are high and decrease with the altitude, with mean values reaching up to 600 Cupressaceae pollen grains m^{-3} for the lowest height and 400 pollen grains m^{-3} for the height range from 90 to 500 m. The wind speed associated with these high pollen concentrations generally remains below 4 m s^{-1} for *all day* periods. Furthermore, there is a contribution from other locations with lower contributions in the eastern side and in the SW direction with average concentrations between 300 and 400 pollen grains m^{-3}. For *non-convective* periods, the days with higher total concentrations consistently show a prevalence of nocturnal winds from the southeastern quadrant across all detected wind speeds. During daytime, in *convective* periods, a higher average concentration of Cupressaceae pollen grains at the center of the bivariate polar plot is observed across any height range, where any favorable wind direction and the wind speed is lower than 3 m s^{-1}. Moreover, when the wind speed exceeds 8 m s^{-1} from SE, they show average concentrations of 300-400 pollen grains m^{-3} in the range of 90 to 150 m above the surface. This value decreases at the other height ranges.

4.2.2. Spearman correlations for Cupressaceae

All height ranges display similar results, with a clear absence of correlation between Cupressaceae pollen concentrations and *w* (Table 4). With respect to v_h, it reaches statistical significance in each of the study scenarios, showing a consistent negative correlation coefficient with values up to -0.40 during *convective* periods. Continuing with the ε, a very similar situation to the previous variable can be observed. However, some differences exist, including the absence of statistical significance in the height range from 90 to 500 m during *non-convective* periods, and an overall stronger correlation compared to other variables. This variable shows the highest correlation coefficient reaching a value of -0.47 for the lowest height range and *convective* period. Finally, *sh* is negatively correlated, however it does not show statistical significance for *non-convective* periods and in the mid-range during *all day* periods.

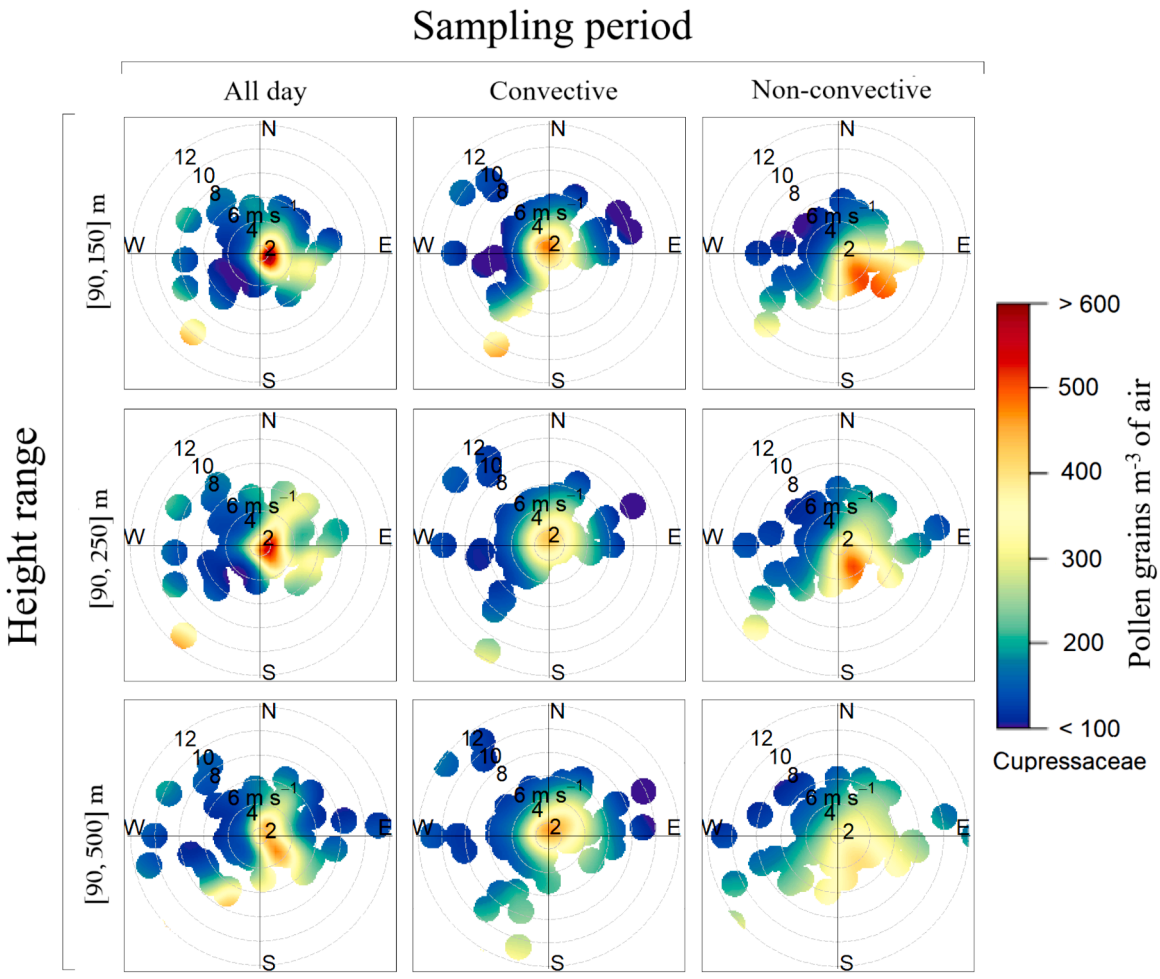

Fig. 4. Bivariate polar plots for the Cupressaceae pollen type at different height ranges and sampling periods. Circles represent horizontal wind speed in m s^{-1}.

Table 4
Spearman correlation coefficients between Cupressaceae daily pollen concentrations and each of the selected variables associated with the ABL dynamics for different height ranges and ABL regimes. Only statistical significant coefficients, i.e. those with a p-value < 0.05, are shown.

	Cupressaceae [90, 150] m				Cupressaceae [90, 250] m				Cupressaceae [90, 500] m			
	v_h	*w*	ε	*sh*	v_h	*w*	ε	*sh*	v_h	*w*	ε	*sh*
All day	-0.37	-	-0.42	-0.15	-0.35	-	-0.36	-	-0.32	-	-0.35	-0.19
Convective	-0.40	-	-0.47	-0.34	-0.40	-	-0.45	-0.30	-0.38	-	-0.41	-0.31
Non-convective	-0.20	-	-0.19	-	-0.23	-	-0.17	-	-0.21	-	-	-

During the *convective* periods, higher correlations are observed which remain nearly constant (around -0.32) across the different height ranges.

4.2.3. GLMs for Cupressaceae

For the variable v_h, stastistical significant negative coefficients appear in some study scenarios, being its influence most clear in the height range from 90 to 250 m (Table 5). Regarding the *w* variable, GLMs enable it to achieve statistical significance. In the lower height range during *non-convective* periods, the positive coefficient implies an additive effect on surface Cupressaceae pollen concentrations. Conversely, *w* shows a negative effect for higher altitude ranges during *convective* periods. With respect to ε, the negative coefficient across all height ranges and during *all day* and *convective* periods indicates that the presence of high turbulence at any altitude within the ABL leads to a reduction in surface Cupressaceae pollen concentrations. Additionally, the model also captures the influence of turbulence in the closest height range to surface during *non-convective* periods. On the other hand, the variable *sh* shows positive effects for *all day* and *non-convective* periods in the lowest height ranges, disagreeing with Spearman's correlations.

Finally, the *dir* variable shows a large number of directions with statistical significance, especially in the lower height range during *all day* and *non-convective* periods. The E direction displays in all cases a positive effect on surface Cupressaceae pollen concentrations. As altitude ranges increase, additional wind directions contribute to this positive effect, with the SE component in the mid-range and NE, SE, and S at the highest altitude range. The rest of the wind directions that reach the statistical significance show a negative effect on Cupressaceae pollen concentration.

Regarding D^2 of each model (Table 5), the highest values are observed for *all day* periods, with percentages between 27% and 37%. In Table 6, it can be observed that most of the variables are involved during *all day* period, presenting statistical significance. The variable *dir* plays a significant contribution in D^2 at any height range, with a maximum value of 17% observed in the lowest height range. Another variable that contributes significantly to D^2 across all height ranges is ε, which increases its influence on surface Cupressaceae pollen concentrations in

Table 5
Sign of the coefficient estimates of the linear predictor when applying a GLM model with Cupressaceae pollen as the response variable and the selected parameters associated with the ABL dynamics as the explanatory variables for different height ranges and ABL regimes. Only statistical significant coefficients, i.e. those with $p < 0.05$ (*), $p < 0.01$ (**) and $p < 0.001$ (***) are presented. The percentage of variance explained, D^2, of each model are also included.

	v_h	w	ε	sh	*dir*								D^2 (%)
					N	NE	E	SE	S	SW	W	NW	
Cupressaceae [90, 150] m													
All day	(-)*	-	(-)***	(+)***	(-)***	(-)*	(+)**	-	(-)*	(-)***	(-)***	(-)***	36.68
Convective	-	-	(-)***	-	-	-	(+)**	-	-	-	-	-	22.60
Non-convective	-	(+)*	(-)**	(+)*	(-)**	(-)***	(+)***	-	(-)***	(-)**	(-)***	(-)***	29.41
Cupressaceae [90, 250] m													
All day	(-)**	-	(-)***	(+)***	(-)**	-	-	-	-	(-)*	(-)*	(-)***	27.35
Convective	(-)*	(-)*	(-)***	-	-	-	(+)***	-	-	-	-	-	21.75
Non-convective	(-)**	-	-	(+)***	(-)*	-	(+)***	(+)**	-	(-)*	(-)**	(-)***	26.96
Cupressaceae [90, 500] m													
All day	-	-	(-)***	-	-	-	(+)**	(+)**	-	-	(-)**	(-)**	25.78
Convective	-	(-)*	(-)***	-	-	-	(+)***	-	-	-	-	-	20.08
Non-convective	(-)*	-	-	-	-	(+)***	(+)***	(+)***	(+)*	-	-	-	24.78

the larger height ranges. In addition, the variables v_h and *sh* present a more limited influence, as demonstrated by their lower contribution to D^2 and their restriction to height ranges from 90 to 250 m. For *convective* periods, the percentages of D^2 ranges between 20% and 23%. In addition, ε is shown as the variable with the highest contribution to D^2, taking values from 7 % to 10%. However, the important contribution of the variable *dir* to the D^2 models is drastically reduced during this period. During *non-convective* periods, the D^2 values range between 25% and 30%, with a continued decrease in D^2 across broader height ranges. The influence of nighttime *dir* on Cupressaceae pollen concentration is much higher than other study periods, showing a maximum value of 21% in the height range closest to the surface. Moreover, the variable *sh* presents a contribution to the D^2 of 5% in the mid-range, where the statistical significance observed in the lowest height range in the GLM output does not persist. The rest of the variables that reach statistical significance, v_h and ε, display very low values of D^2 up to 3% and 2%, respectively.

5. Discussion

The bivariate polar plots indicate that the main source of *Olea* pollen is located some distance from the city in the W-NW sector (Alba et al., 2000), with significant transport occurring during *convective* periods. On the other hand, the primary source of Cupressaceae pollen is within the city in the SE quadrant (Cariñanos et al., 2016b), with a higher contribution to the Cupressaceae pollen concentrations during *non-convective* periods. The high density of each tree species aligns with typical wind patterns in Granada, from the W-NW during the day and E-SE at nights (Ortiz-Amezcua et al., 2022), explaining the observed source locations.

In this study, the *dir* is the variable most influential and important in the transport and dispersion of both pollen types. This result could already be seen in the bivariate plots and, therefore, the GLM analysis confirms that despite the influence of other variables the direction still carries significant weight. Many authors highlight the importance of the surface wind direction in the pollen regional and long-distance transport processes (e.g. Hjelmroos, 1991; Silva Palacios et al., 2000; Rojo et al., 2015). For *Olea* pollen type, the concentrations increase when the wind flows of the main sources at the NW of the city, especially during *convective* periods. The *dir* can explain 27% of the variability of the *Olea* pollen concentrations in the height range for 90 to 500 m, where the model presents the highest D^2 for *Olea* with a value of 29%. This suggest that the *Olea* pollen grains have already been subjected to mixing and dispersion processes before entering the urban ABL at higher altitudes influenced by daytime emissions (Fernández-Rodríguez et al., 2020), well-mixed ABL during convective conditions (Stull, 1988), and prevailing diurnal NW winds. In addition, during the flowering season of *Olea*, stronger upward and downward currents compared to Cupressaceae make its pollen more influenced by ABL vertical movements. Studies have shown that daytime turbulence can transport pollen grains to altitudes of 1-2 km (Helbig et al., 2004; Shang et al., 2020; Robichaud and Comtois, 2021). At night, however, *Olea* pollen concentrations near the surface appears evenly distributed, with no prevailing wind direction affecting concentrations. At night, however, *Olea* pollen concentrations near the surface appears evenly distributed, with no prevailing wind direction affecting concentrations

For Cupressaceae pollen concentrations, the *dir* variable shows significant effects, particularly during *non-convective* periods at any height range, explaining up to the 22% of the variability of the Cupressaceae pollen concentrations. The E direction consistently increases surface concentrations at any moment of the day, influenced by the high density of cypress trees in the eastern part of the city. As the altitude increases, more wind directions, including SE, NE, and S, also contribute positively during nighttime. However, during nighttime and in the lower height ranges, winds originating from the western sector resulted in a reduction in Cupressaceae pollen concentrations due to the lack of sources in those directions.

Table 6
Percentage of D^2 contributing to the model each of the selected variables related to the ABL dynamics obtained by a type II ANOVA test applied to each GLM model. Significance code: $p < 0.05$ (*), $p < 0.01$ (**) and $p < 0.001$ (***).

	Cupressaceae [90, 150] m					Cupressaceae [90, 250] m					Cupressaceae [90, 500] m				
D^2 (%)	v_h	w	ε	sh	*dir*	v_h	w	ε	sh	*dir*	v_h	w	ε	sh	*dir*
All day	**1.71** *	0.25	**4.82** ***	**3.49** ***	**16.70** ***	**2.06** **	0.04	**6.82** ***	**4.07** ***	**10.16** ***	0.06	0.01	**8.98** ***	0.10	**13.29** ***
Convective	0.30	0.66	**7.85** ***	0.08	**3.85** *	**1.65** *	**2.56** **	**6.98** ***	0.20	2.08	0.53	**2.56** **	**9.71** ***	0.21	1.55
Non-convective	0.01	**1.54** *	**1.79** *	1.10	**21.42** ***	**2.89** **	0.05	1.12	**4.47** ***	**18.48** ***	**2.00** *	0.06	0.07	0.74	**19.72** ***

The influence of *w* in each type of pollen is different due to the different flowering periods and the location of the main sources of each one. For *Olea, w* is the other variable that reaches statistical significance. The fact that the emission sources are located outside the city can be the reason for this lack of statistical significance with the other remaining variables. In this case, both GLMs and Spearman correlations are in concordance. During *non-convective* periods, when the *w* is negative (downward air movement), the concentration of *Olea* pollen on the surface increases and vice versa. In stable conditions with reduced turbulence, *w* significantly influences pollen movement, explaining over 5% of surface variability at the height ranges of 90-150 m and 90-500 m. In the middle range, v_h and *sh* become more influential, indicating a shift in ABL dynamics, likely due to the transition between the SBL and the Residual Layer (RL), as well as the possible formation of nocturnal Low-Level Jets (e.g. Banta et al., 2003; Duarte et al., 2015; Pichugina et al., 2017; Tsiringakis et al., 2022).

Despite being lighter than *Olea*, Cupressaceae pollen concentrations do not show a statistically significant correlation with *w* in the Spearman analysis. This can be due to that *w* within the ABL has limited influence on dispersion processes by itself. GLMs, however, reveal a significant influence of *w*, likely through interactions with other variables. The effect of *w* varies between the height range closest to the surface and the other two height ranges. In the lower height range during nighttime, upward air movement (positive *w*) increases Cupressaceae pollen concentrations at surface, explaining about 2% of D^2. This likely occurs due to upward air displacement, caused by the entry of the nocturnal katabatic flow in the ABL of the city (Chemel et al., 2009), which is accompanied by high concentrations of Cupressaceae pollen. Conversely, *w* shows a negative effect for higher altitude ranges during *convective* periods, resulting in concentration increasing as *w* is negative (downward movement), likely due to the high turbulence associated with this period and the lightweight of the pollen grains. In this case, the percentage of D^2 ascend very lightly until 3%.

The Spearman correlation analysis shows a significant negative relationship between v_h and surface Cupressaceae pollen concentrations in all the study scenarios. This indicates that v_h at altitudes within the ABL is closely linked to the transport and dispersion processes of pollen grains when it occurs in the vicinity of the pollen emission source (Hernández-Ceballos et al. 2014; Izquierdo et al. 2017; Bogawski et al., 2019). GLMs also reflect this negative effect but only in specific cases, with the influence most evident at 90 to 250 m, contributing up to 3% to D^2. This variation across different height ranges may be due to the combined influence of v_h and *dir*. The bivariate plot for Cupressaceae shows that higher wind speeds generally bring lower Cupressaceae pollen concentrations, even at night, when winds from primary sources tend to be weaker compared to other directions.

The variable ε reaches statistical significance in all study scenarios for the Spearman correlations, with a strong negative influence, particularly in the lowest height range during *convective* periods (correlation coefficient of -0.47). This highlights the significant role of turbulence in dispersing Cupressaceae pollen throughout the ABL, with an effect that could cover the entire extent of the ABL (e.g. Noh et al., 2013; Sicard et al., 2016). GLMs confirm this effect, with increased turbulence corresponding to lower Cupressaceae pollen concentrations. The ε is the second most influential variable after *dir*, contributing 7% to 10% to D^2, especially during daytime. Cupressaceae pollen, due to its lightweight structure and potential for long-distance transport, responds rapidly to variations in turbulence within the ABL.

Finally, for the variable *sh*, Spearman analysis shows a negative correlation during *all day* and *convective* periods across all height ranges, indicating that *sh* in the CBL reduces surface pollen concentrations. However, GLMs reveal a positive effect on Cupressaceae pollen during *non-convective* periods in the lower height ranges, possibly due to wind shear forming a barrier that traps pollen near the surface (Sun et al., 2012), but these effects should be analyzed separately to extract more robust conclusions. Therefore, it is likely that different effects are being observed in each statistical method. Spearman correlations capture the negative correlation of *sh* across all height ranges during *convective* periods, while the GLMs capture the positive effect during *non-convective* periods, with a more limited scope up to 250 m, and the possible combined effects with other variables.

6. Conclusions

This study underscores the complex relationship between pollen concentrations and ABL dynamics in Granada, Spain, revealing marked differences between *Olea* and Cupressaceae pollen types, due to the different location of their sources and the intrinsic characteristics of the pollen, such as grain weight and flowering period. Statistical models such as GLMs, demonstrated substantial explanatory power considering the crossed relationships between the investigated variables, accounting for up to 37% of variability in Cupressaceae pollen concentrations and 29% in *Olea*. This highlights the importance of including measurements at several heights within ABL, a novel approach given by this study. *Olea* pollen concentrations, primarily transported from cultivated areas outside the city, show a strong dependency on wind direction and vertical wind speed. Conversely, Cupressaceae pollen, which is emitted within city boundaries, shows more correlation between pollen concentration and ABL dynamics. Therefore, the impact of the ABL on surface pollen concentrations varies significantly depending on whether pollen is locally emitted or transported from distant sources. In addition, the local dynamics of the ABL play a crucial role in the transport and dispersion of pollen grains, influenced by winds generated by the topography, diurnal and nocturnal wind patterns, and other factors that influence the local ABL behaviour.

The novelty of correlating atmospheric variables at height in this study paves the way for future research on pollen dynamics, particularly through the inclusion of additional pollen types and other meteorological variables, higher temporal resolution pollen data, and similar analyses conducted in different cities or environments. It demonstrates the need for pollen forecasting models that account for ABL dynamics in order to better predict pollen concentrations, improve public health measures, and optimize urban planning to minimize allergen exposure, especially in areas where pollen sources and ABL dynamics are closely intertwined.

CRediT authorship contribution statement

Juana Andújar-Maqueda: Writing – review & editing, Writing – original draft, Visualization, Software, Methodology, Investigation, Formal analysis, Data curation. **Pablo Ortiz-Amezcua:** Writing – review & editing, Writing – original draft, Visualization, Supervision, Software, Methodology, Investigation, Formal analysis, Data curation, Conceptualization. **Paloma Cariñanos:** Writing – review & editing, Resources, Investigation, Formal analysis, Data curation, Conceptualization. **Jesús Abril-Gago:** Writing – review & editing, Software, Data curation. **Concepción De Linares:** Writing – review & editing, Resources, Funding acquisition, Formal analysis, Data curation. **Gregori de Arruda Moreira:** Writing – review & editing, Software, Funding acquisition. **Juan Antonio Bravo-Aranda:** Writing – review & editing, Software, Data curation. **María José Granados-Muñoz:** Writing – review & editing, Data curation. **Lucas Alados-Arboledas:** Writing – review & editing, Resources, Project administration, Investigation, Funding acquisition, Data curation. **Juan Luis Guerrero-Rascado:** Writing – review & editing, Writing – original draft, Supervision, Resources, Project administration, Methodology, Investigation, Funding acquisition, Data curation, Conceptualization.

Declaration of competing interest

The authors declare that they have no known competing financial interests or personal relationships that could have appeared to influence

the work reported in this paper.

Acknowledgements

This work was supported by the projects INTEGRATYON[3] (PID2020-117825GB-C21 and PID2020-117825GB-C22) and ELPIS (PID2020-120015RB-I00) funded by MCIN/AEI/10.13039/501100011033, by Junta de Andalucía through projects MORADO (C-366-UGR23) and DEM3TRIOS (A-RNM-430-UGR20) and AEROFOUR (C-EXP-167-UGR23), by University of Granada Plan Propio through Excellence Research Unit Earth Science and Singular Laboratories AGORA (LS2022-1) and UCBA-UGR (LS2024-3) program and the project PP2022.PP.34, by projects BIOD22_001 and BIOD22_002, funded by Consejería de Universidad, Investigación e Innovación and Gobierno de España and Unión Europea – NextGenerationEU, by the European Union's Horizon 2020 research and innovation program through projects ACTRIS.IMP (grant agreement No 871115) and ATMO-ACCESS (grant agreement number 101008004) and the strategic network ACTRIS-Spain (RED2022-134824-E). Authors acknowledge the COST Action PROBE (CA18235) for the exchange of expertise. Jesús Abril-Gago received funding through the grant FPU 21/01436, funded by MCIN/AEI/10.13039/501100011033. Funding for open access charge: Universidad de Granada/CBUA.

Data availability

Data will be made available on request.

References

Ahmed, N.I., Thompson, C., Bolnick, D.I., Stuart, Y.E., 2017. Brain morphology of the threespine stickleback (G asterosteus aculeatus) varies inconsistently with respect to habitat complexity: A test of the Clever Foraging Hypothesis. Ecology and Evolution 7 (10), 3372–3380. https://doi.org/10.1002/ece3.2918.

Alba, F., de la Guardia, C.D., Sabariego, S., 2000. Aerobiología en Andalucía: estación de Granada (1999). Red Española de Aerobiología 6, 31–34.

Alarefi, A., Alhusaini, N., Wang, X., Tao, R., Rui, Q., Gao, G., Pang, L., Qiu, B., Zhang, X., 2022. Alcohol dependence inpatients classification with GLM and hierarchical clustering integration using fMRI data of alcohol multiple scenario cues. Experimental Brain Research 240 (10), 2595–2605. https://doi.org/10.1007/s00221-022-06447-y.

AEMET, 2024. Climate Statistics. Granada Airport (1981-2010). Agencia Estatal de Meteorología, Gobierno de España. Retrieved from. http://www.aemet.es/es/portada.

Banta, R.M., Pichugina, Y.L., Newsom, R.K., 2003. Relationship between low-level jet properties and turbulence kinetic energy in the nocturnal stable boundary layer. Journal of the atmospheric sciences 60 (20), 2549–2555. https://doi.org/10.1175/1520-0469(2003)060≤2549:RBLJPA≥2.0.CO;2.

Beggs, P.J., 2015. Environmental Allergens: from Asthma to Hay Fever and Beyond. Current Climate Change Reports 1 (3), 176–184. https://doi.org/10.1007/S40641-015-0018-2.

Bielory, L., Lyons, K., Goldberg, R., 2012. Climate change and allergic disease. Current allergy and asthma reports 12, 485–494. https://doi.org/10.1007/s11882-012-0314-z.

Bohlmann, S., Shang, X., Vakkari, V., Giannakaki, E., Leskinen, A., Lehtinen, K.E.J., Pätsi, S., Komppula, M., 2021. Lidar depolarization ratio of atmospheric pollen at multiple wavelengths. Atmospheric Chemistry and Physics 21 (9), 7083–7097. https://doi.org/10.5194/acp-21-7083-2021.

Borque, P., Luke, E., Kollias, P., 2016. On the unified estimation of turbulence eddy dissipation rate using Doppler cloud radars and lidars. Journal of Geophysical Research: Atmospheres 121 (10), 5972–5989. https://doi.org/10.1002/2015JD024543.

Borycka, K., Kasprzyk, I., 2018. Hourly pattern of allergenic alder and birch pollen concentrations in the air: Spatial differentiation and the effect of meteorological conditions. Atmospheric Environment 182, 179–192. https://doi.org/10.1016/j.atmosenv.2018.03.048.

Bogawski, P., Borycka, K., Grewling, Ł., Kasprzyk, I., 2019. Detecting distant sources of airborne pollen for Poland: Integrating back-trajectory and dispersion modelling with a satellite-based phenology. Science of the Total Environment 689, 109–125. https://doi.org/10.1016/j.scitotenv.2019.06.348.

Cariñanos, P., Casares-Porcel, M., Quesada-Rubio, J.M., 2014. Estimating the allergenic potential of urban green spaces: A case-study in Granada, Spain. Landscape and urban planning 123, 134–144. https://doi.org/10.1016/j.landurbplan.2013.12.009.

Cariñanos, P., Adinolfi, C., Díaz de la Guardia, C., De Linares, C., Casares-Porcel, M., 2016a. Characterization of allergen emission sources in urban areas. Journal of Environmental Quality 45 (1), 244–252. https://doi.org/10.2134/jeq2015.02.0075.

Cariñanos, P., Casares-Porcel, M., de la Guardia, A.V.D., la Cruz-Márquez, R.D., de la Guardia, C.D., 2016b. Charting trends in the evolution of the La Alhambra forest (Granada, Spain) through analysis of pollen-emission dynamics over time. Climatic change 135, 453–466. https://doi.org/10.1007/s10584-015-1589-6.

Cariñanos, P., Ruiz-Peñuela, S., Valle, A.M., de la Guardia, C.D., 2020. Assessing pollination disservices of urban street-trees: The case of London-plane tree (Platanus x hispanica Mill. ex Münchh). Science of the Total Environment 737, 139722. https://doi.org/10.1016/j.scitotenv.2020.139722.

Cariñanos, P., Foyo-Moreno, I., Alados, I., Guerrero-Rascado, J.L., Ruiz-Peñuela, S., Titos, G., Cazorla, A., Alados-Arboledas, L., de la Guardia, C.D., 2021. Bioaerosols in urban environments: Trends and interactions with pollutants and meteorological variables based on quasi-climatological series. Journal of Environmental Management 282, 111963. https://doi.org/10.1016/j.jenvman.2021.111963.

Cariñanos, P., Guerrero-Rascado, J.L., Valle, A.M., Cazorla, A., Titos, G., Foyo-Moreno, I., Alados-Arboledas, L., de la Guardia, C.D., 2022. Assessing pollen extreme events over a Mediterranean site: Role of local surface meteorology. Atmospheric Environment 272, 118928. https://doi.org/10.1016/j.atmosenv.2021.118928.

Charalampopoulos, A., Lazarina, M., Tsiripidis, I., Vokou, D., 2018. Quantifying the relationship between airborne pollen and vegetation in the urban environment. Aerobiologia 34, 285–300. https://doi.org/10.1007/s10453-018-9513-y.

Chemel, C., Staquet, C., Largeron, Y., 2009. Generation of internal gravity waves by a katabatic wind in an idealized alpine valley. Meteorology and atmospheric physics 103 (1), 187–194. https://doi.org/10.1007/s00703-009-0349-4.

Choi, Y.J., Lee, K.S., Oh, J.W., 2021. The impact of climate change on pollen season and allergic sensitization to pollens. Immunology and Allergy Clinics 41 (1), 97–109. https://doi.org/10.1016/j.iac.2020.09.004.

Comtois, P., Alcazar, P., Néron, D., 1999. Pollen counts statistics and its relevance to precision. Aerobiologia 15, 19–28. https://doi.org/10.1023/A:1007501017470.

Cook, R.D., 1979. Influential observations in linear regression. Journal of the American Statistical Association 74 (365), 169–174.

Córdoba-Jabonero, C., Sicard, M., Ansmann, A., del Águila, A., Baars, H., 2018. Separation of the optical and mass features of particle components in different aerosol mixtures by using POLIPHON retrievals in synergy with continuous polarized Micro-Pulse Lidar (P-MPL) measurements. Atmospheric Measurement Techniques 11 (8), 4775–4795. https://doi.org/10.5194/amt-11-4775-2018.

D'Amato, G., Chong-Neto, H.J., Monge Ortega, O.P., Vitale, C., Ansotegui, I., Rosario, N., Haahtela, T., Galan, C., Pawankar, R., Murrieta-Aguttes, M., Cecchi, L., Bergmann, C., Ridolo, E., Ramon, G., Gonzalez Diaz, S., D'Amato, M., Annesi-Maesano, I., 2020. The effects of climate change on respiratory allergy and asthma induced by pollen and mold allergens. Allergy: European Journal of Allergy and Clinical Immunology 75 (9), 2219–2228. https://doi.org/10.1111/ALL.14476.

Darsow, U., Behrendt, H., Ring, J., 1997. Gramineae pollen as trigger factors of atopic eczema: evaluation of diagnostic measures using the atopy patch test. British Journal of Dermatology 137 (2), 201–207. https://doi.org/10.1046/j.1365-2133.1997.18061889.x.

De Linares, C., Delgado, R., Aira, M.J., Alcazar, P., Alonso-Perez, S., Boi, M., Cariñanos, P., Cuevas, E., Díaz de la Guardia, C., Elvira-Rendueles, Fernández-González, D., Galán, C., Gutiérrez-Bustillo, A.M., Pérez-Badia, R., Rodríguez-Rajo, F. J., Ruíz-Valenzuela, L., Tormo-Molina, R., Trigo, M., Valencia-Barrera, R.M., Valle, A., Belmonte, J., 2017. Changes in the Mediterranean pine forest: pollination patterns and annual trends of airborne pollen. Aerobiologia 33, 375–391. https://doi.org/10.1007/s10453-017-9476-4.

de Weger, L.A., Pashley, C.H., Šikoparija, B., Skjøth, C.A., Kasprzyk, I., Grewling, Ł., Thibaudon, M., Magyar, D., Smith, M., 2016. The long distance transport of airborne Ambrosia pollen to the UK and the Netherlands from Central and south Europe. International journal of biometeorology 60, 1829–1839. https://doi.org/10.1007/s00484-016-1170-7.

del Águila, A., Alcaraz-Segura, D., Martínez-López, J., Postma, T., Alados-Arboledas, L., Zamora, R., Navas-Guzmán, F., 2024. Two decades of high-resolution aerosol product over the Sierra Nevada Mountain region (SE Spain): Spatio-temporal distribution and impact on ecosystems. Atmospheric Research, 107515. https://doi.org/10.1016/j.atmosres.2024.107515.

Després, V.R., Alex Huffman, J., Burrows, S.M., Hoose, C., Safatov, A.S., Buryak, G., Fröhlich-Nowoisky, J., Elbert, W., Andreae, M.O., Pöschl, U., Jaenicke, R., 2012. Primary biological aerosol particles in the atmosphere: A review. *Tellus, Series B: Chemical and Physical Meteorology* 64 (1). https://doi.org/10.3402/tellusb.v64i0.15598.

Díaz De La Guardia, C., Alba, F., de Linares, C., Nieto-Lugilde, D., López Caballero, J., 2006. Aerobiological and allergenic analysis of Cupressaceae pollen in Granada (Southern Spain). Journal of Investigational Allergology and Clinical Immunology 16 (1), 24–33.

Dominici, F., McDermott, A., Daniels, M., Zeger, S.L., Samet, J.M., 2005. Revised analyses of the National Morbidity, Mortality, and Air Pollution Study: mortality among residents of 90 cities. Journal of Toxicology and Environmental Health, Part A 68 (13-14), 1071–1092. https://doi.org/10.1111/j.0006-341X.2000.00352.x.

Dosio, A., de Arellano, J.V.G., Holtslag, A.A., Builtjes, P.J., 2003. Dispersion of a passive tracer in buoyancy-and shear-driven boundary layers. Journal of Applied Meteorology and Climatology 42 (8), 1116–1130. https://doi.org/10.1175/1520-0450(2003)042≤1116:DOAPTI≥2.0.CO;2.

Duarte, H.F., Leclerc, M.Y., Zhang, G., Durden, D., Kurzeja, R., Parker, M., Werth, D., 2015. Impact of nocturnal low-level jets on near-surface turbulence kinetic energy. Boundary-layer meteorology 156 (3), 349–370. https://doi.org/10.1007/s10546-015-0030-z.

Egger, P.H., Staub, K.E., 2016. GLM estimation of trade gravity models with fixed effects. Empirical Economics 50, 137–175. https://doi.org/10.1007/s00181-015-0935-x.

Faegri, K., Kaland, P.E., Krzywinski, K., 1989. Textbook of pollen analysis.

Fernández-Rodríguez, S., Maya-Manzano, J.M., Colín, A.M., Pecero-Casimiro, R., Buters, J., Oteros, J., 2020. Understanding hourly patterns of Olea pollen concentrations as tool for the environmental impact assessment. Science of the Total Environment 736, 139363. https://doi.org/10.1016/j.scitotenv.2020.139363.

Filioglou, M., Leskinen, A., Vakkari, V., O'Connor, E., Tuononen, M., Tuominen, P., Komppula, M., 2023. Spectral dependence of birch and pine pollen optical properties using a synergy of lidar instruments. Atmospheric Chemistry and Physics 23 (16), 9009–9021. https://doi.org/10.5194/acp-23-9009-2023.

Frei, T., Gassner, E., 2008. Climate change and its impact on birch pollen quantities and the start of the pollen season an example from Switzerland for the period 1969-2006. International Journal of Biometeorology 52 (7), 667–674. https://doi.org/10.1007/S00484-008-0159-2.

Frisk, C.A., Apangu, G.P., Petch, G.M., Adams-Groom, B., Skjøth, C.A., 2022. Atmospheric transport reveals grass pollen dispersion distances. Science of the Total Environment 814, 152806. https://doi.org/10.1016/j.scitotenv.2021.152806.

Fröhlich-Nowoisky, J., Kampf, C.J., Weber, B., Huffman, J.A., Pöhlker, C., Andreae, M. O., Lang-Yona, N., Burrows, S.M., Gunthe, S.S., Elbert, W., Su, H., Hoor, P., Thines, E., Hoffmann, T., Després, V.R., Pöschl, U., 2016. Bioaerosols in the Earth system: Climate, health, and ecosystem interactions. Atmospheric Research 182. https://doi.org/10.1016/j.atmosres.2016.07.018.

Galán, C., Cariñanos, P., Alcázar, P., Domínguez, E., 2007. Spanish Aerobiology Network (REA): management and quality manual, 184. Servicio de publicaciones de la Universidad de Córdoba, pp. 1–300.

Galán, C., Smith, M., Thibaudon, M., Frenguelli, G., Oteros, J., Gehrig, R., Berger, U., Clot, B., Brandao, R., 2014. Pollen monitoring: minimum requirements and reproducibility of analysis. Aerobiologia 30, 385–395. https://doi.org/10.1007/s10453-014-9335-5335-5.

Garratt, J.R., 1994. The atmospheric boundary layer. Earth-Science Reviews 37 (1-2), 89–134. https://doi.org/10.1016/0012-8252(94)90026-4.

Goldberg, C., Buch, H., Moseholm, L., Weeke, E.R., 1988. Airborne pollen records in Denmark, 1977–1986. Grana 27 (3), 209–217. https://doi.org/10.1080/00173138809428928.

Gottardini, E., Cristofolini, F., Cristofori, A., Vannini, A., Ferretti, M., 2009. Sampling bias and sampling errors in pollen counting in aerobiological monitoring in Italy. Journal of Environmental Monitoring 11 (4), 751–755. https://doi.org/10.1039/b818162b.

Griffin, D.W., 2007. Atmospheric movement of microorganisms in clouds of desert dust and implications for human health. Clinical Microbiology Reviews 20 (3), 459–477. https://doi.org/10.1128/CMR.00039-06.

Guitart-Masip, M., Salami, A., Garrett, D., Rieckmann, A., Lindenberger, U., Bäckman, L., 2016. BOLD variability is related to dopaminergic neurotransmission and cognitive aging. Cerebral Cortex 26 (5), 2074–2083. https://doi.org/10.1093/cercor/bhv029.

Halt, J.A., Silva, B.B., Kawatra, S.K., 2015. A new on-line method for predicting iron ore pellet quality. Mineral Processing and Extractive Metallurgy Review 36 (6), 377–384. https://doi.org/10.1080/08827508.2015.1004403.

Helbig, N., Vogel, B., Vogel, H., Fiedler, F., 2004. Numerical modelling of pollen dispersion on the regional scale. Aerobiologia 20 (1), 3–19. https://doi.org/10.1023/B:AERO.0000022984.51588.30.

Hernández-Ceballos, M.A., Skjøth, C.A., García-Mozo, H., Bolívar, J.P., Galán, C., 2014. Improvement in the accuracy of back trajectories using WRF to identify pollen sources in southern Iberian Peninsula. International journal of biometeorology 58, 2031–2043. https://doi.org/10.1007/s00484-014-0804-x.

Hirst, J., 1952. An automatic volumetric spore trap. Annals of applied Biology 39 (2), 257–265. https://doi.org/10.1111/j.1744-7348.1952.tb00904.x.

Hjelmroos, M., 1991. Evidence of long-distance transport of *betula* pollen. Grana 30 (1), 215–228. https://doi.org/10.1080/00173139109427802.

Hurtado, P., Prieto, M., Aragón, G., de Bello, F., Martínez, I., 2020. Intraspecific variability drives functional changes in lichen epiphytic communities across Europe. Ecology 101 (6), e03017. https://doi.org/10.1002/ecy.3017.

Illingworth, A.J., Hogan, R.J., O'connor, E.J., Bouniol, D., Brooks, M.E., Delanoë, J., Donovan, D.P., Eastment, J.D., Gaussiat, N., Goddard, J.W.F., Haeffelin, M., Klein Baltink, H., Krasnov, O.A., Pelon, J., Piriou, J.M., Protat, A., Russchenberg, H.W.J., Seifert, A., Tompkins, A.M., Van Zadelhoff, G.J., Vinit, F., Willen, U., Wilson, D.R., Wrench, C.L., 2007. Cloudnet: Continuous evaluation of cloud profiles in seven operational models using ground-based observations. Bulletin of the American Meteorological Society 88 (6), 883–898. https://doi.org/10.1175/BAMS-88-6-883.

Izquierdo, R., Alarcon, M., Periago, C., Belmonte, J., 2015. Is long range transport of pollen in the NW Mediterranean basin influenced by Northern Hemisphere teleconnection patterns? Science of the Total Environment 532, 771–779. https://doi.org/10.1016/j.scitotenv.2015.06.047.

Izquierdo, R., Alarcón, M., Mazón, J., Pino, D., De Linares, C., Aguinagalde, X., Belmonte, J., 2017. Are the Pyrenees a barrier for the transport of birch (Betula) pollen from Central Europe to the Iberian Peninsula? Science of the total environment 575, 1183–1196. https://doi.org/10.1016/j.scitotenv.2016.09.192.

Janizadeh, S., Bateni, S.M., Jun, C., Im, J., Pai, H.T., Band, S.S., Mosavi, A., 2023. Combination four different ensemble algorithms with the generalized linear model (GLM) for predicting forest fire susceptibility. Geomatics, Natural Hazards and Risk 14 (1), 2206512. https://doi.org/10.1080/19475705.2023.2206512.

Kolmogorov, A.N., 1941. The local structure of turbulence in incompressible viscous fluid for very large Reynolds' Numbers. *Dokl. Akad. Nauk SSSR* 30, 301.

Kasprzyk, I., Ortyl, B., Dulska-Jeż, A., 2014. Relationships among weather parameters, airborne pollen and seed crops of Fagus and Quercus in Poland. Agricultural and Forest Meteorology 197, 111–122. https://doi.org/10.1016/j.agrformet.2014.05.015.

Kuparinen, A., Markkanen, T., Riikonen, H., Vesala, T., 2007. Modeling air-mediated dispersal of spores, pollen and seeds in forested areas. Ecological modelling 208 (2-4), 177–188. https://doi.org/10.1016/j.ecolmodel.2007.05.023.

Laj, P., Lund Myhre, C., Riffault, V., Amiridis, V., Fuchs, H., Eleftheriadis, E., Petäjä, T., Kivekäs, N., Juurola, E., Saponaro, G., Philippin, S., Cornacchia, C., Alados Arboledas, L., Baars, H., Claude, A., De Mazière, M., Dils, B., Murberg, L.-E., Fiebig, M., Haeffelin, M., Herrmann, H., Höhler, K., Illmann, N., Kreuter, A., Ludewig, E., Marinou, E., Möhler, O., Mona, L., Nicolae, D., O'Connor, E., Petracca Altieri, R.-M., Picquet-Varrault, B., Pospichal, B., Putaud, J.-P., Reimann, S., Salameh, T., Siomos, N., Stachlewska, I., van Pinxteren, D., Voudouri, K.-A., Wandinger, U., Wiedensohler, A., Apituley, A., Comerón, A., Gysel-Beer, M., Mihalopoulos, N., Nikolova, N., Pietruczuk, A., Sauvage, S., Sciare, J., Skov, S., Svendby, T., Swietlicki, E., Tonev, D., Vaughan, G., Zdimal, V., Baltensperger, U., Doussin, J.-F., Kulmala, M., Pappalardo, G., Sorvari Sundet, S., Vana, M., 2024. Aerosol, Clouds and Trace Gases Research Infrastructure–ACTRIS, the European research infrastructure supporting atmospheric science. Bulletin of the American Meteorological Society. https://doi.org/10.1175/BAMS-D-23-0064.1.

Liu, C., Fedorovich, E., Huang, J., 2018. Revisiting entrainment relationships for shear-free and sheared convective boundary layers through large-eddy simulations. Quarterly Journal of the Royal Meteorological Society 144 (716), 2182–2195. https://doi.org/10.1002/QJ.3330.

Liu, C., Huang, J., Wang, Y., Tao, X., Hu, C., Deng, L., Xu, J., Xiao, H.W., Luo, L., Xiao, H. Y., Xiao, W., 2020. Vertical distribution of PM2.5 and interactions with the atmospheric boundary layer during the development stage of a heavy haze pollution event. Science of The Total Environment 704, 135329. https://doi.org/10.1016/J.SCITOTENV.2019.135329.

López, P., Cariñanos, P., 2020. Caracterización de las fuentes de emisión de bioaerosoles (polen de ciprés) en la ciudad de Granada. Bachelor Dissertation. Degree in Environmental Sciences. University of Granada.

Majeed, H.T., Periago, C., Alarcón, M., Belmonte, J., 2018. Airborne pollen parameters and their relationship with meteorological variables in NE Iberian Peninsula. Aerobiologia 34, 375–388. https://doi.org/10.1007/s10453-018-9520-z.

Manninen, A.J., Marke, T., Tuononen, M., O'Connor, E.J., 2018. Atmospheric boundary layer classification with Doppler lidar. Journal of Geophysical Research: Atmospheres 123 (15), 8172–8189. https://doi.org/10.1029/2017JD028169.

Manninen, A., 2019. HALO lidar toolbox. GitHub. Retrieved June 18, 2024, from. https://github.com/manninenaj/HALO_lidar_toolbox.

Mohanty, R.P., Buchheim, M.A., Anderson, J., Levetin, E., 2017. Molecular analysis confirms the long-distance transport of Juniperus *ashei* pollen. PLoS One 12 (3), e0173465. https://doi.org/10.1371/journal.pone.0173465.

Montávez, J.P., Rodríguez, A., Jiménez, J.I., 2000. A study of the urban heat island of Granada. International Journal of Climatology: A Journal of the Royal Meteorological Society 20 (8), 899–911. https://doi.org/10.1002/1097-0088(20000630)20:8≤899::AID-JOC433≥3.0.CO;2-I.

Naclerio, R.M., 1991. Allergic rhinitis. New England Journal of Medicine 325 (12), 860–869. https://doi.org/10.1056/NEJM199109193251206.

Negral, L., Moreno-Grau, S., Galera, M.D., Elvira-Rendueles, B., Costa-Gómez, I., Aznar, F., Pérez-Badia, R., Moreno, J.M., 2021. The effects of continentality, marine nature and the recirculation of air masses on pollen concentration: Olea in a Mediterranean coastal enclave. Science of the Total Environment 790, 147999. https://doi.org/10.1016/j.scitotenv.2021.147999.

Newsom, R.K., Brewer, W.A., Wilczak, J.M., Wolfe, D.E., Oncley, S.P., Lundquist, J.K., 2017. Validating precision estimates in horizontal wind measurements from a Doppler lidar. Atmospheric Measurement Techniques 10 (3), 1229–1240. https://doi.org/10.5194/amt-10-1229-2017.

Noh, Y.M., Müller, D., Lee, H., Choi, T.J., 2013. Influence of biogenic pollen on optical properties of atmospheric aerosols observed by lidar over Gwangju, South Korea. Atmospheric Environment 69, 139–147. https://doi.org/10.1016/j.atmosenv.2012.12.018.

O'Connor, E.J., Illingworth, A.J., Brooks, I.M., Westbrook, C.D., Hogan, R.J., Davies, F., Brooks, B.J., 2010. A method for estimating the turbulent kinetic energy dissipation rate from a vertically pointing Doppler lidar, and independent evaluation from balloon-borne in situ measurements. Journal of atmospheric and oceanic technology 27 (10), 1652–1664. https://doi.org/10.1175/2010JTECHA1455.1.

Ortiz-Amezcua, P., Martínez-Herrera, A., Manninen, A.J., Pentikäinen, P.P., O'Connor, E. J., Guerrero-Rascado, J.L., Alados-Arboledas, L., 2022. Wind and Turbulence Statistics in the Urban Boundary Layer over a Mountain–Valley System in Granada, Spain. Remote Sensing 14 (10), 2321. https://doi.org/10.3390/RS14102321.

Päschke, E., Leinweber, R., Lehmann, V., 2015. An assessment of the performance of a 1.5 µm Doppler lidar for operational vertical wind profiling based on a 1-year trial. Atmospheric Measurement Techniques 8 (6), 2251–2266. https://doi.org/10.5194/amt-8-2251-2015.

Pentikäinen, P., O'Connor, E.J., Manninen, A.J., Ortiz-Amezcua, P., 2020. Methodology for deriving the telescope focus function and its uncertainty for a heterodyne pulsed Doppler lidar. Atmospheric Measurement Techniques 13 (5), 2849–2863. https://doi.org/10.5194/amt-13-2849-2020.

Pichugina, Y.L., Brewer, W.A., Banta, R.M., Choukulkar, A., Clack, C.T.M., Marquis, M. C., McCarty, B.J., Weickmann, A.M., Sandberg, S.P., Marchbanks, R.D., Hardesty, R. M., 2017. Properties of the offshore low level jet and rotor layer wind shear as measured by scanning Doppler Lidar. Wind Energy 20 (6), 987–1002. https://doi.org/10.1002/we.2075.

Prospero, J.M., Blades, E., Mathison, G., Naidu, R., 2005. Interhemispheric transport of viable fungi and bacteria from Africa to the Caribbean with soil dust. Aerobiologia 20 (2), 99–110. https://doi.org/10.1007/s10453-004-5872-7.

Rachmawati, R.N., Sari, A.C., Yohanes, 2021. Lasso Regression for Daily Rainfall Modeling at Citeko Station, Bogor, Indonesia. Procedia Computer Science 179, 383–390. https://doi.org/10.1016/j.procs.2021.01.020.

Ren, Y., Zhang, H., Zhang, X., Wei, W., Li, Q., Wu, B., Cai, X., Song, Y., Kang, L., Zhu, T., 2021. Turbulence barrier effect during heavy haze pollution events. Science of the Total Environment 753, 142286. https://doi.org/10.1016/j.scitotenv.2020.142286.

Robichaud, A., Comtois, P., 2021. Numerical modelling of birch pollen dispersion in Canada. Environmental Research 194, 110554. https://doi.org/10.1016/j.envres.2020.110554.

Rojo, J., Rapp, A., Lara, B., Fernández-González, F., Pérez-Badia, R., 2015. Effect of land uses and wind direction on the contribution of local sources to airborne pollen. Science of the Total environment 538, 672–682. https://doi.org/10.1016/j.scitotenv.2015.08.074.

Roy, P., Chen, L.W.A., Chen, Y.T., Ahmad, S., Khan, E., Buttner, M., 2023. Pollen Dispersion and Deposition in Real-World Urban Settings: A Computational Fluid Dynamic Study. Aerosol Science and Engineering 7 (4), 543–555. https://doi.org/10.1007/s41810-023-00198-1.

Saha, S., Saha, A., Hembram, T.K., Mandal, K., Sarkar, R., Bhardwaj, D., 2022. Prediction of spatial landslide susceptibility applying the novel ensembles of CNN, GLM and random forest in the Indian Himalayan region. Stochastic Environmental Research and Risk Assessment 36 (10), 3597–3616. https://doi.org/10.1007/s00477-022-02212-3.

Santos-Alamillos, F.J., Pozo-Vázquez, D., Ruiz-Arias, J.A., Tovar-Pescador, J., 2015. Influence of land-use misrepresentation on the accuracy of WRF wind estimates: Evaluation of GLCC and CORINE land-use maps in southern Spain. Atmospheric Research 157, 17–28. https://doi.org/10.1016/j.atmosres.2015.01.006.

Santiago, J.L., Martín, F., Martilli, A., 2013. A computational fluid dynamic modelling approach to assess the representativeness of urban monitoring stations. Science of the total environment 454, 61–72. https://doi.org/10.1016/j.scitotenv.2013.02.068.

Schmidt, C.W., 2016. Pollen overload: Seasonal allergies in a changing climate. Environmental Health Perspectives 124 (4), A71–A75. https://doi.org/10.1289/EHP.124-A70.

Shang, X., Giannakaki, E., Bohlmann, S., Filioglou, M., Saarto, A., Ruuskanen, A., Leskinen, A., Romakkaniemi, S., Komppula, M., 2020. Optical characterization of pure pollen types using a multi-wavelength Raman polarization lidar. Atmospheric Chemistry and Physics 20 (23), 15323–15339. https://doi.org/10.5194/acp-20-15323-2020.

Shang, X., Baars, H., Stachlewska, I.S., Mattis, I., Komppula, M., 2022. Pollen observations at four EARLINET stations during the ACTRIS-COVID-19 campaign. Atmospheric Chemistry and Physics 22 (6), 3931–3944. https://doi.org/10.5194/acp-22-3931-2022.

Shi, Y., Liu, L., Hu, F., Fan, G., Huo, J., 2021. Nocturnal boundary layer evolution and its impacts on the vertical distributions of pollutant particulate matter. Atmosphere 12 (5). https://doi.org/10.3390/atmos12050610.

Sicard, M., Izquierdo, R., Alarcón, M., Belmonte, J., Comerón, A., Baldasano, J.M., 2016. Near-surface and columnar measurements with a micro pulse lidar of atmospheric pollen in Barcelona, Spain. Atmospheric Chemistry and Physics 16 (11), 6805–6821. https://doi.org/10.5194/acp-16-6805-2016.

Silva, L., 2014. A feature engineering approach to wind power forecasting: GEFCom 2012. International Journal of Forecasting 30 (2), 395–401. https://doi.org/10.1016/j.ijforecast.2013.07.007.

Silva Palacios, I., Tormo Molina, R., Muñoz Rodríguez, A.F., 2000. Influence of wind direction on pollen concentration in the atmosphere. International Journal of Biometeorology 44, 128–133. https://doi.org/10.1007/s004840000059.

Stull, R.B., 1988. An introduction to boundary layer meteorology, 13. Springer Science & Business Media. Vol.

Sun, J., Mahrt, L., Banta, R.M., Pichugina, Y.L., 2012. Turbulence regimes and turbulence intermittency in the stable boundary layer during CASES-99. Journal of the Atmospheric Sciences 69 (1), 338–351. https://doi.org/10.1175/JAS-D-11-082.1.

Trigo, M.D.M., Jato, V., Fernández, D., Galán, C., 2008. Atlas aeropalinológico de España. Secretariado de publicaciones de la Universidad de Leon, España.

Tsiringakis, A., Theeuwes, N.E., Barlow, J.F., Steeneveld, G.J., 2022. Interactions between the nocturnal low-level jets and the urban boundary layer: a case study over London. Boundary-Layer Meteorology 183 (2), 249–272. https://doi.org/10.1007/s10546-021-00681-7.

Van Vliet, A.J., Overeem, A., De Groot, R.S., Jacobs, A.F., Spieksma, F.T., 2002. The influence of temperature and climate change on the timing of pollen release in the Netherlands. International *Journal of Climatology: A Journal of the Royal Meteorological Society* 22 (14), 1757–1767. https://doi.org/10.1002/joc.820.

Vakkari, V., O'connor, E.J., Nisantzi, A., Mamouri, R.E., Hadjimitsis, D.G., 2015. Low-level mixing height detection in coastal locations with a scanning Doppler lidar. Atmospheric Measurement Techniques 8 (4), 1875–1885. https://doi.org/10.5194/amt-8-1875-2015875-2015.

Veselovskii, I., Hu, Q., Goloub, P., Podvin, T., Choël, M., Visez, N., Korenskiy, M., 2021. Mie–Raman–fluorescence lidar observations of aerosols during pollen season in the north of France. Atmospheric Measurement Techniques 14 (7), 4773–4786. https://doi.org/10.5194/amt-14-4773-2021.

Wahid, N.A.A., Suhaila, J., Rahman, H.A., 2021. The influence of climate factors on hand-foot-mouth disease: A five-state study in Malaysia. Universal Journal of Public Health 9 (5), 324–331. https://doi.org/10.13189/ujph.2021.090515.

Wei, W., Zhang, H., Cai, X., Song, Y., Bian, Y., Xiao, K., Zhang, H., 2020. Influence of intermittent turbulence on air pollution and its dispersion in winter 2016/2017 over Beijing, China. Journal of Meteorological Research 34 (1), 176–188. https://doi.org/10.1007/S13351-020-9128-4.

Weichle, T., Hynes, D.M., Durazo-Arvizu, R., Tarlov, E., Zhang, Q., 2013. Impact of alternative approaches to assess outlying and influential observations on health care costs. Springerplus 2 (1), 614. https://doi.org/10.1186/2193-1801-2-614.

Zeldin, D.C., Eggleston, P., Chapman, M., Piedimonte, G., Renz, H., Peden, D., 2006. How exposures to biologics influence the induction and incidence of asthma. Environmental health perspectives 114 (4), 620–626. https://doi.org/10.1289/ehp.8379.

Zhang, Y., Zhang, Y., Yu, C., Yi, F., 2021. Evolution of aerosols in the atmospheric boundary layer and elevated layers during a severe, persistent haze episode in a central China megacity. Atmosphere 12 (2), 152. https://doi.org/10.3390/atmos12020152.

Zhou, W., Fleming, E., Legendre, G., Roux, L., Latreille, J., Gendronneau, G., Oh, J., 2023. Skin microbiome attributes associate with biophysical skin ageing. Experimental dermatology 32 (9), 1546–1556. https://doi.org/10.1111/exd.14863.